JACS
JOURNAL OF THE AMERICAN CHEMICAL SOCIETY
pubs.acs.org/JACS

Article

Kinetic Modeling of the Reversible or Irreversible Electrochemical Responses of FeFe-Hydrogenases

Andrea Fasano, Carole Baffert, Conrad Schumann, Gustav Berggren, James A. Birrell, Vincent Fourmond, and Christophe Léger*

Cite This: J. Am. Chem. Soc. 2024, 146, 1455−1466

ABSTRACT: The enzyme FeFe-hydrogenase catalyzes H_2 evolution and oxidation at an active site that consists of a [4Fe-4S] cluster bridged to a $[Fe_2(CO)_3(CN)_2$(azadithiolate)] subsite. Previous investigations of its mechanism were mostly conducted on a few "prototypical" FeFe-hydrogenases, such as that from *Chlamydomonas reinhardtii*(Cr HydA1), but atypical hydrogenases have recently been characterized in an effort to explore the diversity of this class of enzymes. We aim at understanding why prototypical hydrogenases are active in either direction of the reaction in response to a small deviation from equilibrium, whereas the homologous enzyme from *Thermoanaerobacter mathranii* (Tam HydS) shows activity only under conditions of very high driving force, a behavior that was referred to as "irreversible catalysis". We follow up on previous spectroscopic studies and recent developments in the kinetic modeling of bidirectional reactions to investigate and compare the catalytic cycles of Cr HydA1 and Tam HydS under conditions of direct electron transfer with an electrode. We compare the hypothetical catalytic cycles described in the literature, and we show that the observed changes in catalytic activity as a function of potential, pH, and H_2 concentration can be explained with the assumption that the same catalytic mechanism applies. This helps us identify which variations in properties of the catalytic intermediates give rise to the distinct "reversible" or "irreversible" catalytic behaviors.

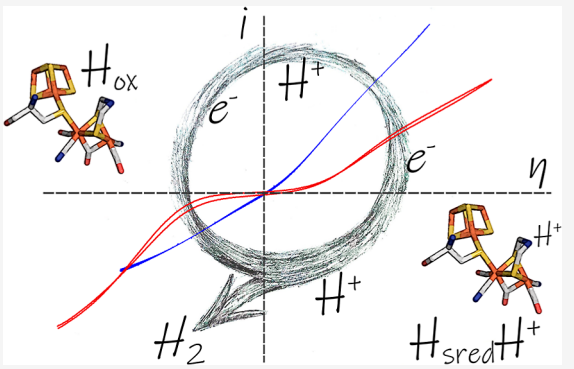

INTRODUCTION

The redox reactions of H_2 oxidation and production are catalyzed in Nature by metalloenzymes whose active sites are composed of abundant metals, Ni and Fe, and are called hydrogenases. Here, we focus on FeFe-hydrogenases, whose active site, called the "H-cluster", is composed of a $[4Fe\text{-}4S]_H$ cluster, linked by a cysteine to a dinuclear Fe center ($[2Fe]_H$). The two Fe ions of $[2Fe]_H$ are coordinated by three carbonyl ligands (one of which is bridging) and two cyanides and bridged by an amine-dithiolate (ADT) ligand. The Fe ion that is remote from the cubane is referred to as the "distal" Fe, or Fe_d. In the catalytic cycle, H_2 binds to the open coordination site on Fe_d, and it is split heterolytically into a terminal hydride and a proton. The latter binds to the nitrogen of the ADT ligand,[1,2] from where it is transferred to a nearby cysteine, and then further along a chain of acidic residues.[3,4] This proton-transfer pathway is very conserved in the phylogenetic group of FeFe-hydrogenases that includes the most studied enzymes (called group "A", or "prototypical" in ref 5). In these enzymes, long-range electron transfer may involve accessory FeS clusters.

Detailed information about the catalytic cycle has been obtained over decades of spectroscopic investigations. Some of the proposed catalytic intermediates are paramagnetic and hence detectable by electron paramagnetic resonance spectroscopy, but the spectroscopic technique that has become the most popular in hydrogenase research is Fourier transform infrared (FTIR) spectroscopy, which can detect the vibrations of the CO and CN diatomic ligands to identify various states of the H-cluster. Regarding prototypical hydrogenases, two distinct mechanistic hypotheses have emerged.[6]

The most oxidized catalytic intermediate is H_{ox}, where the electronic configuration of the dinuclear cluster is Fe(II)/Fe(I) and the cubane is oxidized (2+). In model 1 (Figure 1D), the reduction of H_{ox} at high pH produces the H_{red} state, where the cubane is reduced. H_{red} has a pK_a value around 7, and at pH < pK_a, the reduction of H_{ox} is coupled to a protonation, to give the $H_{red}H^+$ state. This protonation was evidenced by the pH dependence of the reduction potential of the H_{ox} state observed in spectroelectrochemical titrations of the active site at different pH values (the corresponding Pourbaix

Received: September 28, 2023
Revised: November 16, 2023
Accepted: December 1, 2023
Published: January 2, 2024

https://doi.org/10.1021/jacs.3c10693
J. Am. Chem. Soc. 2024, 146, 1455−1466

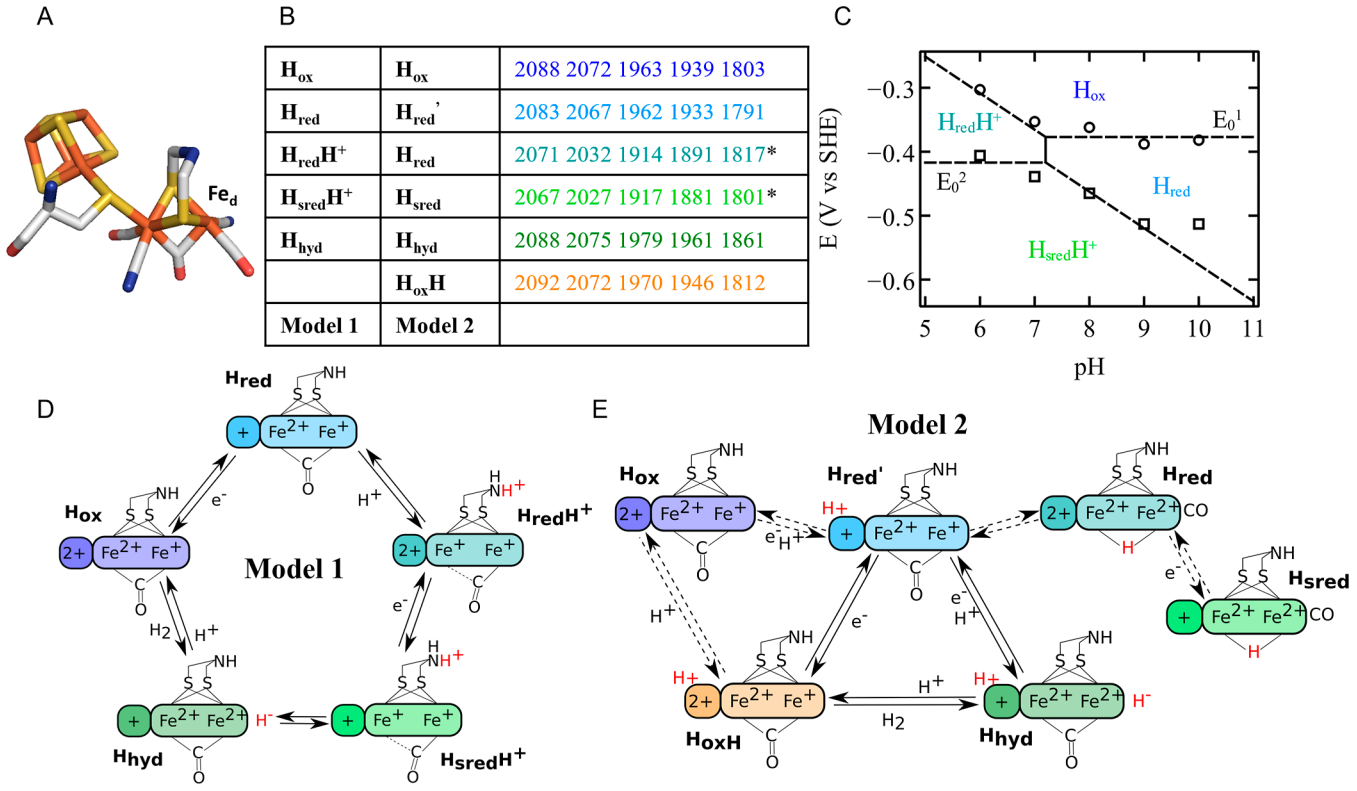

Figure 1. (A) Active site "H-cluster" of [FeFe]-hydrogenases (color code: Fe (orange), S (yellow), C (white), N (blue), and O (red)). (B) FTIR frequencies of the Cr HydA1 states in panels D and E; the states of models 1 and 2 that share the same FTIR signature are shown with the same color. Asterisks on the vibration frequencies of $H_{red}H^+$ and $H_{sred}H^+$ mark the bridging CO frequencies detected at low temperature in ref 7. (C) Pourbaix diagram of H_{ox}, H_{red}, $H_{red}H^+$, and $H_{sred}H^+$ transitions adapted from ref 8; (D) model 1 of the catalytic cycle of [FeFe]-hydrogenases, proposed in ref 8; and (E) model 2 of the catalytic cycle of [FeFe]-hydrogenases, proposed in ref 9.

diagram is reproduced from ref 8 in Figure 1C). The vibrational band of the bridging CO ligand is apparently lost upon protonation, suggesting that the ligand shifts to a terminal position.[10,11] However, recent data suggests that the band is only weak and highly broadened, as low-temperature measurements produce a more intense sharp band.[7,12,13] It is hypothesized that binding of the proton to the nitrogen of the amine in the azadithiolate ligand induces an intramolecular electron transfer from the cubane to the dinuclear cluster, which becomes Fe(I)/Fe(I). An increased electron density at $[2Fe]_H$ explains the larger red shift of the vibration bands in the H_{ox} to $H_{red}H^+$ transition than in H_{ox} to H_{red}.[8] Reduction of $H_{red}H^+$ gives the super-reduced state $H_{sred}H^+$,[14] with a protonated amine and a reduced cubane, which is a tautomer of H_{hyd}, with a hydride on Fe_d.[15−18] The second protonation of the doubly reduced state gives a series of elusive species, called $H_{hyd}H^+$ and $H_{ox}H_2$, from which the release of H_2 completes the catalytic cycle by giving back H_{ox}. Some spectroscopic signatures have been attributed to $H_{hyd}H^+$.[16,19]

In model 2 (Figure 1E), the FTIR signature assigned to the H_{red} state is instead attributed to a state called H_{red}' (panel E), and the H_{ox} to H_{red}' reaction supposedly involves the reduction and coupled protonation of the cubane. This was concluded from the pH dependence of the potential of the cubane, measured in enzyme variants where the nitrogen atom of the amine dithiolate bridge is replaced with a carbon atom.[20] (However, this observation was recently challenged.[21]) Consistent with the above-described transformation between H_{red} and $H_{red}H^+$, H_{red}' is replaced at pH below 7 with the $H_{red}H^+$ state, which is called H_{red} in model 2 (Figure 5C in ref 9). However, at variance with model 1, it is assumed that the transition from H_{red}' to H_{red} at low pH is the result of a proton rearrangement, with a deprotonation of the cubane and the formation of a bridging hydride, and the bridging CO shifts to an apical position (something that is not supported by the spectroscopic investigations of Cr in ref 13, and not observed in any of the states of the H-cluster of *Clostridium acetobutylicum* hydrogenase I[12]). Considering the expected stability of this bridging hydride, the H_{red} species and the corresponding H_{sred} state obtained by further reduction (which has the same spectroscopic signature as the species denoted as $H_{sred}H^+$ in model 1) are considered to be off-pathway. Instead, reductive catalysis proceeds from H_{red}', whose one-electron one-proton reduction gives a hydride species also denoted as H_{hyd} but now considered protonated on the cubane in addition to Fe_d. The so-called "regulatory" proton on the cubane is retained throughout the catalytic cycle. Further steps of reduction, protonation, and H_2 release give back H_{red}' bypassing the H_{ox} state, which is also considered off-pathway (see Figure 2 of ref 9). Whether or not the spectroscopic signal assigned to $H_{ox}H$ reflects a true catalytic intermediate or an artifact is currently debated.[22,23]

Recently, two FeFe-hydrogenases whose active site environment differs significantly from that in group A have been characterized, although to a much lesser extent than for group A hydrogenases. These enzymes are*Thermotoga maritima* (Tm) HydS[24] and*Thermoanaerobacter mathranii* (Tam) HydS,[25] from groups C and D, respectively.[26] Albeit from two distinct phylogenetic groups, the latter enzymes feature an identical set of electron relay FeS clusters and are structurally

https://doi.org/10.1021/jacs.3c10693
J. Am. Chem. Soc. 2024, 146, 1455−1466

very similar. Indeed, as compared to group A enzymes, most of the altered amino acids in the direct vicinity of the H-cluster are identical in *Tam* HydS and *Tm* HydS. In the sequences of both enzymes, the cysteine residue that accepts protons from the amine dithiolate ligand in group A hydrogenases is replaced with an alanine, and none of the residues that form the proton-transfer pathway in group A hydrogenases are present; a possible alternative pathway was recently identified in group D.[27] The strong similarities between Tam HydS and Tm HydS suggest similar active site properties and function.

In Tm HydS, the H_{ox} FTIR signature is very similar to that of group A hydrogenases (compare Figure 1B and Figure 5A in ref 24), but the midpoint potentials of the two one-electron redox transitions are more separated than those of Cr HydA1 (−300 and −570 mV in Tm HydS[24] vs −362 and −465 mV in Cr HydA1,[8] both at pH 8), suggesting that the half-reduced state of the H-cluster is stable over a larger potential range in Tm HydS than in Cr HydA1. How this is determined by the environment of the H-cluster is unclear.[28] Regarding Tam HydS, the H_{ox} state signature is again unremarkable, and, as is the case with Tm, the one-electron reduced state is very stable.[25]

In terms of functional properties, both Tam and Tm HydS have low activity (consistent with their putative role as H_2 sensors), but Tam HydS is also remarkable in that catalysis is only observed upon application of a large driving force for H_2 oxidation or evolution, and we assume that this is also the case for Tm HydS. This behavior, termed "irreversible catalysis",[29−32] is observed in voltammetric experiments where the enzyme undergoes direct electron transfer with an electrode and catalysis is detected as a positive or negative current (for H_2 oxidation and evolution, respectively), as the electrode potential is shifted from the Nernst potential of the H^+/H_2 couple.[33,34] In the particular case of Tam HydS, we ruled out the possibility that this irreversibility is the consequence of slow interfacial electron transfer or results from the catalytic cycle being different in the two directions of the reaction,[31] but the relation between irreversible catalysis and the details of the catalytic cycle still needs to be established.

Here, we follow up on recent advances in the kinetic modeling of bidirectional catalytic voltammetry[35−40] to propose an original point of view on the catalytic cycle of prototypical and atypical FeFe-hydrogenases. We aim at giving a full description of how the voltammogram shapes (catalytic potentials and limiting currents) depend on pH and H_2 concentration. Our analysis of the voltammetry of Cr HydA1 appears to be fully consistent with model 1 and gives further information about the thermodynamic properties of the reduced catalytic intermediates. The Tam HydS voltammetric data can be analyzed assuming that the same catalytic mechanism is operational, and this helps us identify variations in properties of the catalytic intermediates that make the two enzymes behave "reversibly" and "irreversibly".

RESULTS

pH Titration of Cr HydA1. We recorded Cr HydA1 FTIR spectra at different pH values, from 5 to 10, at a constant H_2 partial pressure (2% H_2 in N_2, P_{tot} = 1 atm), under equilibrium conditions. In this series of experiments, the enzyme was diluted from a concentrated stock solution into a buffer of the desired pH, so that the concentration of enzymes was always the same. Each experiment was performed in triplicate.

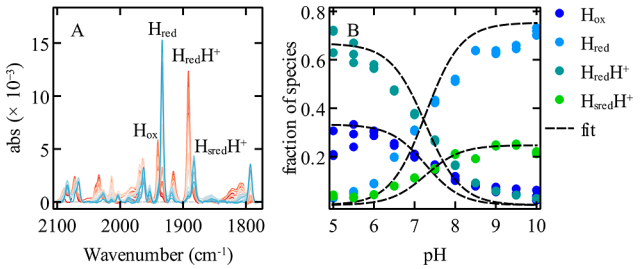

Figure 2. Cr HydA1 pH titration at 2% H_2. (A) Overlay of the FTIR spectra baseline subtracted as a function of pH (from 5 (red) to 10 (blue)). (B) Fit of the fraction of states H_{ox}, H_{red}, $H_{red}H^+$, and $H_{sred}H^+$ (same color code as in Figure 1) with the model proposed in ref 8 (Supporting Information Section S1.2), giving the following parameters: pK = 7.2, E_1^0 = −359 mV, and E_2^0 = −405 mV vs SHE. Each data point was measured in triplicate; the dispersion of the results is visible in panel B.

Figure 2A shows the spectral transition of Cr HydA1 from a high pH (blue) to a low pH (red). We have monitored the intensities of the bands of H_{ox} (1939 cm^{-1}) and $H_{red}H^+$ (1891 cm^{-1}), mostly present at low pH, and of H_{red} (1933 cm^{-1}) and $H_{sred}H^+$ (1881 cm^{-1}), mostly present at high pH.[8] The H_{hyd} state was omitted because the corresponding band at around 1850 cm^{-1} was too small to be reliably quantified.

The sum of the intensities of the peaks corresponding to these four main states was constant across pH values (see Figure S1.1). We explain in Supporting Information Section S1.1 how we calculated the fractions of these species shown as a function of pH in Figure 2B, with the same color code as in Figure 1. By changing the pH at a constant H_2 pressure, we also change the potential experienced by the enzyme at each pH value, as described by the Nernst equation. This allowed us to fit the model proposed in ref 8 to the data, considering two redox reactions, H_{ox}/H_{red} and $H_{red}H^+/H_{sred}H^+$, whose reduction potentials $E_1^{0\prime}$ and $E_2^{0\prime}$ depend on pH (as described in eqs 7 and 8 below), and one protonation whose acidity dissociation constant K defines the relative populations of H_{red} and $H_{red}H^+$. This model can be fitted to the fractions of H_{ox}, H_{red}, $H_{red}H^+$, and $H_{sred}H^+$ as a function of pH (black dashed lines in Figure 2B, see the equations in Supporting Information Section S1.2) by adjusting three parameters: the alkaline limit of $E_1^{0\prime}$, −359 mV vs SHE, the acidic limit of $E_2^{0\prime}$, −405 mV, and the value of pK, 7.2. All these values are close to those previously measured from the results of spectroelectrochemical experiments.[8]

These data show that a very similar behavior of the Cr HydA1 enzyme is observed under thermodynamic equilibrium in a pH titration as has been observed previously in pseudoequilibrium spectroelectrochemical titrations (ref 8). Moreover, these data, when analyzed with an appropriate thermodynamic model, provide the relevant pK_a values and redox potentials that can be compared to those derived in kinetic modeling of electrochemistry data, vide infra.

Further analysis of the spectroscopy of Tam HydS will be helpful to fully elucidate the relation between the structures and IR signatures. In the recent pioneering work on Tam HydS, a large hysteresis in the titration of the active site prevented the measurement of thermodynamic parameters.[25] In combination with the limited number of H-cluster states identified in Tam HydS to date, we chose not to perform the pH titration of Tam HydS in this work, leaving it for future investigations.

https://doi.org/10.1021/jacs.3c10693
J. Am. Chem. Soc. 2024, 146, 1455−1466

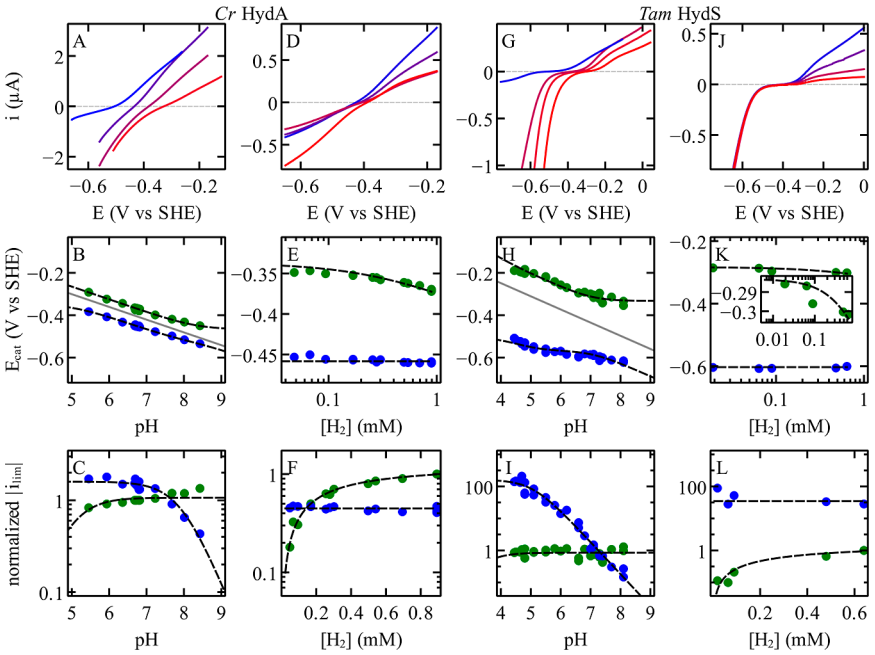

Figure 3. Cyclic voltammograms, catalytic potentials, and limiting currents at different pHs and $[H_2]$ pressures for Cr HydA1 and Tam HydS. The black dashed lines are the best fits of eqs 11−14, with the parameters shown in Table 1 (deduced from the analysis of voltammetry at different pH values) or the best fits of eqs 23 and 26, with the parameters shown in Table 2 (from the analysis of voltammetry at different $[H_2]$ concentrations). Panels A and D show selected blank subtracted, averaged, cyclic voltammograms for Cr HydA1 at different pH values (under 1 atm of $[H_2]$, 30 °C) and $[H_2]$ pressures (at pH 7.7, 5 °C), respectively. Colors go from blue to red from high to low pH (pH values are 5.4, 6.3, 7.2, and 8.4 in panel A) and from high to low H_2 partial pressure (0.89, 0.36, 0.18, and 0.04 mM $[H_2]$ in panel D). Other conditions: scan rate 20 mV/s and electrode rotation rate 3000 rpm. Panels G and J show selected, blank subtracted, averaged cyclic voltammograms for Tam HydS at different pH values (under 1 atm of $[H_2]$, 40 °C) and $[H_2]$ pressures (at pH 6.5, 40 °C), respectively. Colors go from blue to red from high to low pH (pH values are 4.8, 5.5, 6, and 8.1 in panel G) and from high to low H_2 partial pressure (0.64, 0.5, 0.09, and 0.06 mM $[H_2]$ in panel J). Other conditions: 10 mV/s and 3000 rpm. The catalytic potentials and the normalized limiting currents are plotted as functions of pH (panels B and C for Cr HydA1 and panels H and I for Tam HydS) and as functions of H_2 concentration (panels E and F for Cr HydA1 and panels K and L for Tam HydS). The current values were normalized by the value of i_{lim}^{ox} at pH 7 in the plots of i_{lim} against pH and by the value of i_{lim}^{ox} under 1 atm. of H_2 in the plots of i_{lim} against $[H_2]$. In green E_{cat}^{ox} and i_{lim}^{ox} and in blue E_{cat}^{red} and i_{lim}^{red}. In panels B and H, a solid gray line indicates the Nernst potential of the H^+/H_2 couple.

Voltammetry. We examined the catalytic responses of Cr HydA1 and Tam HydS adsorbed onto the surface of a PGE electrode under conditions of direct electron transfer.[33,34] We recorded cyclic voltammograms at a slow scan rate (so that the obtained current response is always under steady state), rotating and rotated the electrode at a fast rate so that mass transport of the substrate H_2 toward the electrode is not influential. Recording a single voltammogram gives little information about the catalytic cycle (just like the measurement of a single value of the catalytic rate in a solution assay), but we examined how the steady-state current response depends on pH at a constant H_2 pressure (1 atm.) and on the concentration of H_2 (changed by changing the partial H_2 pressure) at a constant pH (pH 6.5 for Tam HydS and 7.7 for Cr HydA1).

The steady-state catalytic responses of hydrogenases are analyzed here (and in all of our previous work) with a generic rate equation that depends on four parameters: two limiting currents i_{lim}^{ox} and i_{lim}^{red} whose values are proportional to the turnover frequency under very oxidizing and very reducing conditions and two "catalytic potentials" E_{cat}^{ox} and E_{cat}^{red}.[35,37,41]

$$i = \frac{i_{lim}^{ox} \exp^{F(E-E_{cat}^{ox})/RT} \exp^{F(E-E_{cat}^{red})/RT} - i_{lim}^{red}}{1 + \exp^{F(E-E_{cat}^{red})/RT}(1 + \exp^{F(E-E_{cat}^{ox})/RT})} \quad (1)$$

The catalytic potentials are the values of the electrode potential below and above which H_2 evolution and oxidation, respectively, are observed. They are measured from the positions of the inflection potentials of the catalytic waves, or by fitting a model to the waveshape.[35,37,41] By definition, irreversible catalysis corresponds to the situation where E_{cat}^{ox} is significantly greater than E_{cat}^{red}, with a potential range where no catalysis occurs.[29−31,37]

The rate equation must be modified to account for the broadening that results from slow and distributed interfacial electron transfer, as described previously.[35,42] For this, we assume that electron transfer between the electrode and the active site is direct and that the values of the ET rate constants depend on electrode potential according to the Butler−Volmer equation. This is correct for Cr HydA1, which embeds no accessory clusters, and it is also a good approximation in the case of Tam HydS (despite the probable implication of FeS clusters in mediating long-range electron transfer in this enzyme) on condition that intramolecular electron transfer is fast relative to the turnover of Tam HydS.[35] Considering slow intramolecular electron transfer would add parameters to a model that already provides a very good fit of the data, so these parameters would necessarily be underdetermined.[35]

The model was then fitted to the voltammograms (see Sections S2.7−S2.9 and ref 31) to measure the catalytic potentials and the high and low potential limiting currents. The latter are related to the equilibrium potential (the Nernst potential of the H^+/H_2 couple) by the following equation[37]

https://doi.org/10.1021/jacs.3c10693
J. Am. Chem. Soc. 2024, 146, 1455−1466

$$\frac{i_{\lim}^{ox}}{i_{\lim}^{red}} = \exp\left[\frac{2F}{RT}\left(\frac{E_{cat}^{ox} + E_{cat}^{red}}{2} - E_{eq}\right)\right] \quad (2)$$

The steady-state rate equation (eq 1) and the constraint in eq 2 are valid for the steady-state voltammetric response of any two-electron bidirectional catalytic cycle that is "ordered" (meaning that it involves the same series of steps for the forward and backward reactions).[37] Since the rate equation does not depend on the details of the catalytic cycle such as the order of the catalytic steps, the only conclusion from the observation that the equation fits well the voltammetry is that the catalytic mechanism is ordered. However, important insights come from the detailed interpretation of how the four parameters (catalytic potentials and limiting currents) depend on the experimental parameters, in particular pH and H_2 concentration, as discussed in ref 40 and illustrated below.

MODELING

The meaning of the catalytic potentials depends on the order and the rate constants of the steps in the catalytic cycle,[37] and to interpret the dependence of the catalytic potentials and limiting currents on pH and H_2 concentration, one has to make explicit assumptions about which rate constants depend on pH and $[H_2]$.[40] A kinetic model that would involve all of the steps that have been postulated in the catalytic cycle of FeFe-hydrogenases would depend on too many parameters and would be impractical from the point of view of the kinetic analysis. Like in a recent study of H^+/H_2 conversion by a synthetic complex,[39] the compromise that we found useful was to consider a catalytic cycle model that includes four distinct steps: two redox steps ("E") and two nonredox steps ("C" for "chemical"), as depicted in Figure 4A.

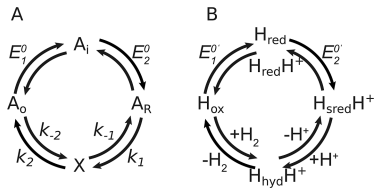

Figure 4. Kinetic schemes discussed in this paper. (A) Generic scheme of the catalytic mechanism EECC,[1] where A is the active site (in the redox states O, oxidized, I, intermediate, and R, reduced), "X" is a catalytic intermediate, and all steps are reversible. (B) Mechanism adapted to analyze the steady-state kinetics of hydrogenases. The two-electron reduction of H_{ox} to $H_{sred}H^+$ is coupled to one protonation (hence the pH dependence of $E_1^{0\prime}$ and $E_2^{0\prime}$ in eqs 7 and 8), and the first and second chemical steps correspond to protonation (eqs 9 and 10) and H_2 release/binding (eqs 21 and 22), so that the "X" intermediate corresponds to $H_{hyd}H^+$ and $H_{ox}H_2$. Only the former is shown in (B).

The limiting currents and catalytic potentials depend on the values of E_1^0 and E_2^0 and on the values of the four rate constants of the two chemical steps, as demonstrated in ref 37

$$i_{\lim}^{ox} = 2FA\Gamma\frac{k_{-1}k_{-2}}{k_2 + k_{-1} + k_{-2}} \quad (3)$$

$$i_{\lim}^{red} = -2FA\Gamma\frac{k_1k_2}{k_1 + k_2 + k_{-1}} \quad (4)$$

$$E_{cat}^{ox} = E_1^0 - \frac{RT}{F}\ln\frac{k_2 + k_{-1} + k_{-2}}{k_2 + k_{-1}} \quad (5)$$

$$E_{cat}^{red} = E_2^0 + \frac{RT}{F}\ln\frac{k_2 + k_{-1} + k_1}{k_2 + k_{-1}} \quad (6)$$

To match the mechanism of model 1 and the Pourbaix diagram in Figure 1C, we assume that the first redox step (the reduction of H_{ox}) is coupled to a fast protonation at pH < pK, so that its redox potential depends on pH according to

$$E_1^{0\prime} = E_1^0 + \frac{RT}{F}\ln\left[1 + \frac{[H^+]}{K}\right] \quad (7)$$

where pK is the pK_a of H_{red} (corresponding to the protonation of the amine bridge) and E_1^0 is the reduction potential of the H_{ox}/H_{red} couple in the alkaline limit, as indicated in Figure 1C. As a consequence, the redox potential of the second redox step is

$$E_2^{0\prime} = E_2^0 - \frac{RT}{F}\ln\left[1 + \frac{K}{[H^+]}\right] \quad (8)$$

where E_2^0 is the reduction potential of the $H_{red}H^+/H_{sred}H^+$ couple in the acidic limit. These two redox steps correspond to the two-electron, one-proton reduction of H_{ox} into $H_{sred}H^+$ (Figure 1A).

The reductive catalytic cycle is completed by a series of chemical steps that include the second protonation, and H_2 binding and release, which we describe in the model by two distinct, bidirectional, nonredox steps "C" (Figure 4A).

A strong assumption is that the $H_{red}/H_{red}H^+$ transition is fast on the turnover time scale and remains at equilibrium during the catalytic cycle, whereas the second protonation is allowed to be slow. This reduces the catalytic cycle to just four steps. This approximation is given justification by the very good agreement between the resulting "EECC" model in Figure 4A and the data, as described below. Making the first protonation also slow (in what would become an "ECECC" scheme) would add parameters to a model that is already very good, so these parameters would necessarily be underdetermined (the situation is the same as that discussed above, regarding our rudimentary description of the electron-transfer kinetics). In our attempts to find the "best" and simplest model, we have also considered an ECEC catalytic cycle, which failed to reproduce the pH dependence (cf. Section S2.10).

pH Dependence of the Cr HydA1 Voltammetric Response. We first focus on the pH dependence of the catalytic potentials and limiting currents of Cr HydA1. For this, we explicitly include a protonation in the first chemical step as shown in Figure 4B using a realistic description of the (de)protonation kinetics (we also tested protonation in step 2, but this leads to inconsistencies; cf. Section S2.1). Since the proton is transferred to the H-cluster from the final proton relay (the side chain of a conserved cysteine residue in group A hydrogenases) rather than directly from bulk water or from the buffer, the rate constants of the protonation and deprotonation steps, k_1 and k_{-1}, respectively, depend on the pH according to

$$k_1 = \frac{k_1^{max}}{1 + \frac{K_{relay}}{[H^+]}} \quad (9)$$

$$k_{-1} = \frac{k_{-1}^{max}}{1 + \frac{[H^+]}{K_{relay}}} \quad (10)$$

where K_{relay} is the acidity constant of the proton relay.[39,43]

https://doi.org/10.1021/jacs.3c10693
J. Am. Chem. Soc. 2024, 146, 1455−1466

Replacing E_1^0 and E_2^0 with $E_1^{0\prime}$ and $E_2^{0\prime}$ and substituting eqs 9 and 10 into eqs 3−6 give the pH dependence of the two limiting currents and the two catalytic potentials as a function of eight parameters: K, defined in eqs 7 and 8, E_2^0, defined above, and α, β, E_1^{0app}, K_1, K_2, and K_3, all defined below.

$$i_{lim}^{ox} = \frac{\alpha}{1 + \frac{[H^+]}{K_1}} \tag{11}$$

$$i_{lim}^{red} = \frac{\beta}{1 + \frac{K_3}{[H^+]}} \tag{12}$$

$$E_{cat}^{ox} = E_1^{0app} + \frac{RT}{F}\ln\left[1 + \frac{[H^+]}{K}\right] + \frac{RT}{F}\ln\left[\frac{1 + \frac{[H^+]}{K_2}}{1 + \frac{[H^+]}{K_1}}\right] \tag{13}$$

$$E_{cat}^{red} = E_2^0 - \frac{RT}{F}\ln\left[1 + \frac{K}{[H^+]}\right] + \frac{RT}{F}\ln\left[\frac{1 + \frac{[H^+]}{K_3}}{1 + \frac{[H^+]}{K_2}}\right] \tag{14}$$

The parameters α and β in eqs 11 and 12 are pH independent

$$\alpha = 2FA\Gamma\frac{k_{-2}k_{-1}^{max}}{k_2 + k_{-2} + k_{-1}^{max}} \tag{15}$$

$$\beta = -2FA\Gamma\frac{k_2k_1^{max}}{k_2 + k_1^{max}} \tag{16}$$

They are not discussed further because their value defines the magnitude of the voltammetric current, which, in Protein Film Electrochemistry, is proportional to the unknown electroactive coverage, Γ, and thus cannot be interpreted.[33,44] Four of the six parameters in eqs 11−14 are related to the parameters of the catalytic cycle by the following relations

$$E_1^{0app} = E_1^0 + \frac{RT}{F}\ln\left[\frac{k_2 + k_{-1}^{max}}{k_2 + k_{-2} + k_{-1}^{max}}\right] \tag{17}$$

$$K_1 = K_{relay} \times \frac{k_2 + k_{-2} + k_{-1}^{max}}{k_2 + k_{-2}} \tag{18}$$

$$K_2 = K_{relay} \times \frac{k_2 + k_{-1}^{max}}{k_2} \tag{19}$$

$$K_3 = K_{relay} \times \frac{k_2 + k_{-1}^{max}}{k_2 + k_1^{max}} \tag{20}$$

pK_1, pK_2, and pK_3 are "catalytic pK_a's",[40] which depend on the acidity of the proton relay and on kinetic parameters. These apparent pK_a's defined by eqs 18−20 are not thermodynamic quantities (as explained in ref 40). They do not each correspond to the protonation of a particular intermediate, but they are three because a model that includes three protonation events (here, two at the active site and one at the proton relay) should depend on at most three apparent pK_a's. Similarly, the value of E_1^{0app} cannot be easily interpreted because it is shifted from E_1^0, the alkaline limit of $E_1^{0\prime}$ (cf. eq 17). The other two parameters, E_2^0 and K, are thermodynamic quantities. We used eqs 11−14 to interpret the variations with pH of the catalytic potentials and limiting currents of Cr HydA1 (panels B−F in Figure 3).

Considering eq 11, the observation that i_{lim}^{ox} is pH independent (green data points in Figure 3C) implies pK_1 < 5. The value of pK_3 ≈ 7.9 could, Figure 4, be directly deduced by fitting eq 12 to the pH dependence of i_{lim}^{red} (blue in Figure 3C).

The same apparent acidity constants ("K_i") appear in several of eqs 11−14, meaning that the four variations with pH are not independent of one another. Moreover, eqs 18−20 imply that pK_2 is necessarily lower than both pK_1 and pK_3. This gave useful constraints to interpret the pH dependence of the catalytic potentials.

Fitting eq 14 to the pH dependence of E_{cat}^{red} (green in Figure 3B) using the constraint pK_2 < pK_3 and pK_3 ≈ 7.9 (measured from i_{lim}^{ox}) gave E_2^0 = −523 mV and pK = 8.3 (slightly above the value, 7.2, determined from the data in Figure 2).

Fitting eq 13 to the pH dependence of E_{cat}^{ox} (blue in Figure 3B) with the constraint pK_2 < pK_1 (compare eqs 18 and 19), with pK = 8.3 (from the above fit of the pH dependence of E_{cat}^{red}), and pK_1 < 5 (from the pH dependence of i_{lim}^{ox}) returned E_1^{0app} (which is lower than $E_1^{0\prime}$, cf. eq 17). Although it is difficult to estimate an error on the value of pK, we observed that a value of pK = 7.8 (instead of the best value of 8.3) also gives a fit that is acceptable, with a value of E_1^{0app} that is 30 mV more positive than its best value.

These Cr HydA1 parameters are collected on the first row of Table 1. The values of some of the parameters can only be specified as an upper limit (e.g., pK_1 < 5) because any value lower than that indicated gives an equally good fit of the data.

Table 1. Parameters Obtained by Fitting Eqs 11−14 to the Data Shown in Panels B, C, H and I of Figure 3 to Interpret the pH Dependence of the Catalytic Potentials and Limiting Currents[a]

	E_1^{0app} (mV)	E_2^0 (mV)	pK	pK_1	pK_2	pK_3
Cr HydA1	−466	−523	8.3	<5	<5	7.9
Tam HydS	−332	−568	7.1	<3.5	<4	5.1

[a] E_1^{0app} is distinct from E_1^0 (cf. eq 17).

Dependence on H_2 Concentration of the Cr HydA1 Voltammetric Response. To explain the dependence of the catalytic potentials and limiting currents on $[H_2]$ at a constant pH, we included the binding and release of H_2 in step 2, Figure 4B, assuming for simplicity that the release of H_2 is unimolecular

$$k_2 = \text{cst} \tag{21}$$

and H_2 binding is bimolecular

$$k_{-2} = k'_{-2} \times [H_2] \tag{22}$$

Considering more complex H_2-binding kinetics (as described in Section S2.3) is not useful: it accounts for the slight inhibition by H_2 of H_2 evolution, but it does not change the conclusions of this work while adding to the model parameters that cannot be determined.

Substituting eqs 21 and 22 in eqs 3−6 gave

$$i_{lim}^{ox} = 2FA\Gamma\frac{k_{-1}}{1 + \frac{K_M}{[H_2]}} \tag{23}$$

https://doi.org/10.1021/jacs.3c10693
J. Am. Chem. Soc. 2024, 146, 1455−1466

$$i_{\mathrm{lim}}^{\mathrm{red}} = -2FA\Gamma\frac{k_1k_2}{k_1 + k_2 + k_{-1}} \quad (24)$$

$$E_{\mathrm{cat}}^{\mathrm{ox}} = E_1^{0\prime} - \frac{RT}{F}\ln\left[1 + \frac{[\mathrm{H_2}]}{K_{\mathrm{M}}}\right] \quad (25)$$

$$E_{\mathrm{cat}}^{\mathrm{red}} = E_2^{0\mathrm{app}} = E_2^{0\prime} + \frac{RT}{F}\ln\frac{k_2 + k_{-1} + k_1}{k_2 + k_{-1}} \quad (26)$$

with

$$K_{\mathrm{M}} = \frac{k_2 + k_{-1}}{k'_{-2}} \quad (27)$$

We fitted eqs 23−27 to interpret the dependence of the limiting currents and catalytic potentials recorded at a constant pH on the H_2 concentration.

The reductive limiting current is nearly independent of H_2 (blue in Figure 3F), consistent with eq 24. The change in $i_{\mathrm{lim}}^{\mathrm{ox}}$ against $[H_2]$ (green in Figure 3F and eq 23) returned a value of K_M = 0.3 mM that is consistent with previous measurements of ours.[45]

Equation 26 is consistent with the observation that $E_{\mathrm{cat}}^{\mathrm{red}}$ is independent of H_2 pressure. Fitting a horizontal line to $E_{\mathrm{cat}}^{\mathrm{red}}$ (blue in Figure 3E) gave the value of $E_2^{0\mathrm{app}}$ reported in Table 2, which is offset from the value of $E_2^{0\prime}$ (cf. eq 26).

Equation 25 accounts for the observed decrease in $E_{\mathrm{cat}}^{\mathrm{ox}}$ as the concentration of H_2 increases above the value of K_M (green in Figure 3E). The effect is small because the value of K_M is high (even at the low temperature, 5 °C, that we used in this series of experiments), and it is not possible to record data at H_2 concentrations well above K_M. Yet, the trends are clear and fully consistent with eqs 23−27.

Table 2. Parameters Obtained by Fitting Eqs 23−27 to the Data Shown in Panels E, F, K, and L of Figure 3 to Interpret the Dependence on $[H_2]$ of the Catalytic Potentials and Limiting Currents at pH = 7.7 (Cr HydA1) and 6.5 (Tam HydS)[a]

	$E_1^{0\prime}$ (mV)	$E_2^{0\mathrm{app}}$ (mV)	K_M (mM)
Cr HydA1	−337	−458	0.3
Tam HydS	−283	−603	0.6

[a]The corresponding Cr HydA1 data (Figure 3E,F) were recorded at 5 °C, where the K_M value is lower,[45] and the variations of $E_{\mathrm{cat}}^{\mathrm{ox}}$ and $i_{\mathrm{lim}}^{\mathrm{ox}}$ against H_2 are more clearly seen. Here, the value of parameter $E_2^{0\mathrm{app}}$ is offset from $E_2^{0\prime}$ (cf. eq 26) and thus cannot be interpreted.

Analysis of the Tam Data. We used the same kinetic model, the same assumptions, and the same approach to analyze the "irreversible" voltammograms obtained with the enzyme from Tam HydS (panels G−L in Figure 3). The only difference was that, as explained before,[31] the equilibrium potential was measured using a platinized electrode, and its value was used to constrain the fit (using eq 2) to obtain well-defined values of the catalytic potentials; this was not needed for the Cr HydA1 data because the Cr HydA1 catalytic current sharply crosses the potential axis at $E = E_{\mathrm{eq}}$.

The variations with pH and $[H_2]$ of the limiting currents (panels I and L in Figure 3) are similar to those observed with Cr HydA1 (panels C and F).

The value of K_M is larger than that of Cr HydA1 (cf. Table 2), but this is explained by the Tam HydS experiments being carried out at 40 °C, compared to 5 °C for the dependence on $[H_2]$ of the Cr HydA1 data (a high temperature was required because the activity of Tam HydS and the catalytic currents are small), and the value of K_M increases with temperature.[45] We confirmed this K_M value at 40 °C, measured from the CVs in Figure 3, by the chronoamperometry experiments shown in Supporting Information Section S2.6. The large value of K_M makes the dependence of $E_{\mathrm{cat}}^{\mathrm{ox}}$ on $[H_2]$ in Tam HydS flatter than in Cr HydA1, but the increase in $E_{\mathrm{cat}}^{\mathrm{ox}}$ at low H_2 concentrations is clearly observed (inset in Figure 3K), consistent with eq 25. This cannot be explained by assuming H_2 binding in step 1 (cf. Supporting Information Section S2.2).

Also, the value of pK_3 is significantly lower in Tam HydS than in Cr HydA1 (cf. Table 1) which can be seen from the saturation of the H_2 evolution current below a lower value of the pH, compare panels C and I in Figure 3. For Tam HydS, the value of pK_3 = 5.1 measured from the pH dependence of $i_{\mathrm{lim}}^{\mathrm{red}}$ (blue in Figure 3I) is also clearly seen as an inflection in the pH dependence of $E_{\mathrm{cat}}^{\mathrm{red}}$ (green in Figure 3H). The larger difference between pK and pK_3 in Tam HydS compared to Cr HydA1 (still with values of pK_1 and pK_2 outside the experimental pH range) explains the nonlinear pH dependence of the catalytic potentials seen in Figure 3H.

The K_M value measured here for Tam HydS is close to that measured for other FeFe hydrogenases, despite the putative implication of Tam HydS in sensing rather than catalysis. That the Michaelis constants of FeFe-hydrogenases are apparently all similar contrasts with the situation observed with other series of homologous enzymes: the K_M values of CO-dehydrogenases, for example, range over orders of magnitude.[46] However, a Michaelis constant is a convoluted kinetic parameter (eq 27) whose meaning is not straightforward.

DISCUSSION

Protein film voltammetry gives the dependence of activity on electrochemical driving force, from which "catalytic potentials" can be measured.[37,41] In the case of H^+/H_2 conversion by hydrogenases, these are the values of the electrode potentials below and above which H_2 evolution and oxidation, respectively, are observed. How these values depend on substrate concentration can be interpreted to learn about the sequence of events in the catalytic cycle,[33,47,48] but in the particular case of hydrogenases, that the protonation steps may be slow on the time scale of turnover significantly complicates their interpretation: the catalytic potentials depart from the equilibrium reduction potentials measured in redox titrations.

The catalytic potentials can be measured without making any assumption about the catalytic cycle; however, their values depart from the true (equilibrium) reduction potentials of the active site, and their meaning depends on the details of the catalytic cycle. Similarly, we have shown before that if protonation is slow on the time scale of turnover, the dependence of the catalytic potentials and limiting currents on pH defines apparent pK_a's, which we called "catalytic pK_a's". These pK_a's are kinetic parameters whose interpretation is model dependent.[40] That a catalytic system under steady-state turnover conditions defines apparent parameters (apparent potentials, acidity, or dissociation constants) is not unexpected: it is textbook knowledge that a Michaelis−Menten constant is an apparent dissociation constant that depends on all steps in the catalytic cycle rather than a true thermodynamic parameter.

https://doi.org/10.1021/jacs.3c10693
J. Am. Chem. Soc. 2024, 146, 1455−1466

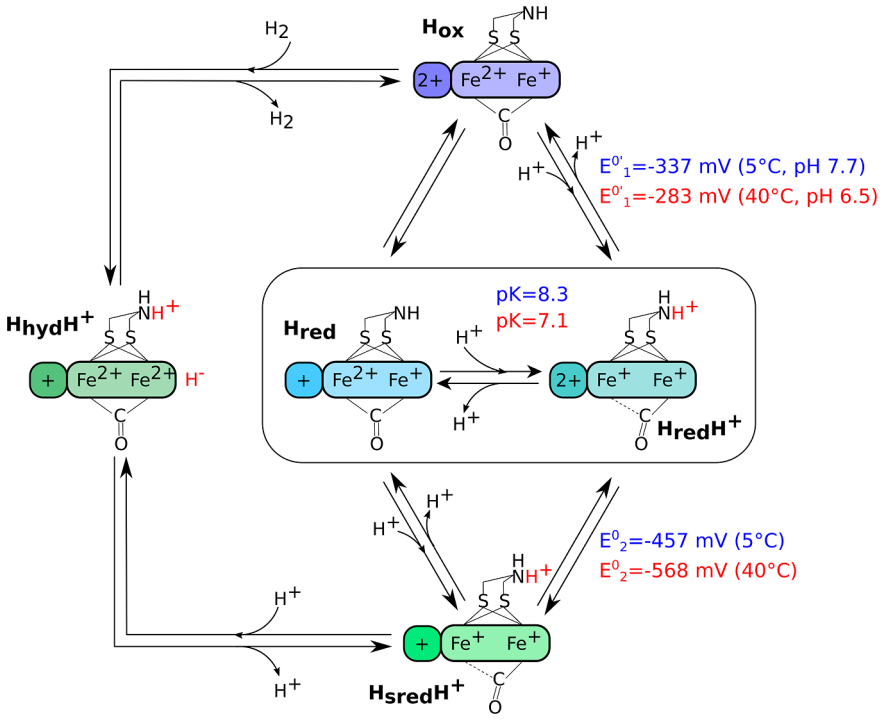

Figure 5. Proposed catalytic cycle for FeFe-hydrogenases. The intermediate states of the catalytic cycle are colored as in Figure 1. The values of $E_1^{0\prime}$, E_2^0, and pK obtained by fitting the voltammetry of Cr HydA1 and Tam HydS at different pH values and H_2 partial pressures are marked on the right side of the figure in blue and red, respectively. The values of $E_1^{0\prime}$ were obtained by the analysis at different H_2 pressures, at a specific pH, reported in the figure. E_2^0 is measured from the analysis at different pHs, and it is the acidic limit of $E_2^{0\prime}$, independent of pH when pH < pK. In the kinetic model, the $H_{red}/H_{red}H^+$ transition (inside the rectangle) is assumed to remain in equilibrium.

Here, we interpreted and compared the variations with pH and H_2 pressure of the catalytic potentials and limiting currents of the "reversible" hydrogenases, Cr HydA1, and the "irreversible" one, Tam HydS, using a kinetic model of catalysis based on the current knowledge of the catalytic cycle (model 1 in Figure 1D). According to this model, the most oxidized H_{ox} state is reduced in two one-electron-transfer steps, one of which is coupled to protonation, and the resulting $H_{sred}H^+$ species undergoes protonation before it releases H_2. Model 2 could not be used to analyze the voltammetric data because the transition from H_{red}' to the low pH inactive branch (H_{red} and H_{sred} in Figure 1E) and from $H_{ox}H$ to the presumably less active H_{ox} state at high pH should induce a decrease in proton reduction activity as the pH is lowered, and a decrease in H_2 oxidation activity as the pH is increased, neither of which are observed under conditions of direct electron transfer (panels C and I in Figure 3). The pH-independent, slow formation of reduced inactive states has been observed in FeFe-hydrogenases, under conditions that are more reducing than those used in this work, but they have not been associated with specific spectroscopic signatures.[49,50]

Interpreting the kinetics of the catalytic cycle in the context of model 1 implies the pH dependences of the reduction potentials of the two ET steps given by eqs 7 and 8 and the dependence on pH and H_2 concentration of the two nonredox steps given by eqs 9, 10, 21, and 22, respectively. Substitution in eqs 3−6 gave relations 11−14 and 23−26, which successfully predict the variations in limiting currents and catalytic potentials as a function of pH at a constant H_2 pressure and as a function of H_2 at a constant pH.

In contrast, considering either protonation in step 2 or H_2 release in step 1 does not give a consistent description of the data. With this hypothesis, eqs 11−14 remain valid, but the meaning of the catalytic pKs and the constraints differ (Supporting Information Section S2.1). Fitting this model to the pH variations of E_{cat} and i_{lim} of Cr HydA1 and Tam HydS returns pK < 5 and pK < 4, respectively. This is not consistent with the value of pK = 7.2 measured in Cr HydA1.[8] A low value of pK is expected if we consider the catalytic cycle of model 2 (without the inactive states, that is, $H_{ox}H$ → unprotonated H_{red}' → H_{hyd} → $H_{ox}H$, solid arrows in Figure 1E); this mechanistic hypothesis may explain the observed dependence on pH of the Cr HydA1 data on condition that H_2 release is in step 1, and protonation in step 2, but then, this model predicts the wrong variation of E_{cat}^{ox} with [H_2] (Supporting Information Section S2.2). Therefore, we were not able to reconcile model 2 with the Cr HydA1 data.

For the same reasons, analysis of the Tam HydS voltammetry gives a pK value for the half-reduced state close to 7. This is not consistent with the spectroscopic investigation of Tm HydS, which did not detect any protonated state of the H-cluster.[24] This will have to be investigated further by examining how the reduction potentials of the active sites of Tm and Tam HydS depend on pH, which is probably the easiest way to detect the coupling between protonation and reduction, which is assumed in our kinetic model and which necessarily occurs in the catalytic cycle of hydrogenases.

Regarding the analysis of the Cr HydA1 data, the parameters that we deduced by fitting eqs 11−14 and 23−26 (Tables 1 and 2, respectively) are consistent with the results of previous investigations: the pK_a value of the one-electron reduced state (pK ≈ 8.3) is close enough to that measured in redox titrations (7.2 in ref 8) and pH titrations (pK around 7.5 in Figure 5C of ref 9 and 7.2 from the data in Figure 2); the value of K_M also

https://doi.org/10.1021/jacs.3c10693
J. Am. Chem. Soc. 2024, 146, 1455−1466

matches to previous chronoamperometric measurements.[45] It is not possible to deduce the alkaline limit E_1^0 from the analysis of the pH dependence of the catalytic potentials because it is shifted from the value of the parameter that we can measure, E_1^{0app}, cf. eq 17. However, the analysis of the dependence on H_2 concentration at a constant pH gives the value of $E_1^{0\prime}$ at pH = 7.7, −337 mV, which matches the value of −362 mV at pH 8 in ref 8 (this value is confirmed from the analysis of the data in Figure 2). The acidic limit of $E_2^{0\prime}$ obtained from the analysis of the voltammetry at different pH values (E_2^0 = −523 mV at 30 °C, Table 1) is lower than the value of −417 mV at 15 °C measured in ref 8 and −405 mV at room temperature from the equilibrium FTIR data in Figure 2. However, the reduction potentials are temperature dependent, and the analysis of the pH dependence of the voltammetry at 5 °C gives E_2^0 = −457 mV (Supporting Information Section S2.5), which we consider close enough to the results of the spectroscopic titrations.

Regarding Tam HydS, there are no available results of equilibrium titrations that we could compare to the values of E_2^0 in Table 1 and $E_1^{0\prime}$ in Table 2 since the titration in Figure S8 of ref 25 shows a very strong hysteresis that attests to a strong departure from equilibrium. However, the titration of Tm HydS in ref 24 is consistent with the larger thermodynamic stability of $H_{red}/H_{red}H^+$ that we detect in Tam HydS: the result of the titration gave $E_1^{0\prime}$ = −300 and $E_2^{0\prime}$ = −570 mV in Tm HydS at pH 8 [24], while the analysis of the voltammetry of Tam HydS returns $E_1^{0\prime}$ = −283 at pH 6.5 (Table 2) and E_2^0 (the acidic limit of $E_2^{0\prime}$) = −568 mV (Table 1).

We assumed that the same mechanism applies in Cr HydA1 and Tam HydS (Figure 5), but their catalytic waveshapes are different, and so are the parameters that we measured from the analyses of the variations with pH and H_2 of their catalytic potentials and limiting currents. These differences between Cr HydA1 and Tam HydS are all consistent with an increased irreversibility of the catalytic response in Tam HydS compared to Cr HydA1 (i.e., a larger separation between the oxidative and reductive catalytic potentials).

Our data show that the half-reduced catalytic intermediate (considering both H_{red} and $H_{red}H^+$) is stable over a range of potential that is about 165 mV larger in Tam HydS than in Cr HydA1, which results from both E_1^0 being more positive in Tam HydS than in Cr HydA1 and E_2^0 being more negative (Tables 2 and 1, respectively). This thermodynamic stability of the half-reduced state contributes to making the catalytic response of Tam HydS very irreversible.

In contrast, the unstable nature of the half-reduced active site is a key feature of bidirectional reversible catalysts.[32,37] The difference $E_1^{0\prime} - E_2^{0\prime}$ is indeed less positive in Cr HydA1 than in Tam HydS, and even negative in the case of two recently described bidirectional reversible synthetic catalysts. The +1 redox state of the $[Pt(depe)_2][PF_6]_2$ (depe = 1,2-bis-(diethylphosphino)ethane) complex that converts CO_2 and formate in acetonitrile is inherently unstable, and the reduction of $[Pt(depe)_2]^{2+}$ is therefore a cooperative two-electron process.[51,52] The recent investigation of the $[Ni(P_2^{Cy}N_2^{Arg})_2]^{6+}$ Dubois complex that reversibly converts H^+ and H_2[30,53] also showed that the reduction potential of the $Ni^{II}/Ni^{I}H^+$ couple is much lower than that of the more reduced $Ni^{III}H^-/Ni^{II}H^-$ couple, which makes the half-reduced tautomers $Ni^{I}H^+$ and $Ni^{III}H^-$ unstable.[39] In both cases, therefore, potential inversion[54] destabilizes the half-reduced form of the active site and thus decreases $E_{cat}^{ox} - E_{cat}^{red}$ and contributes to make the response reversible.

Another difference between the two hydrogenases can be seen as a lower value of pK_3 in Tam HydS compared to Cr HydA1 (Table 1), which contributes to a decrease in E_{cat}^{red} (cf. eq 14). Considering the definition of K_3 in eq 20, the lower value of pK_3 can be interpreted in two different manners. One explanation is that the proton-transfer relay has lower pK_a (the acidity constant is "K_{relay}" in eqs 18−20), which is consistent with the recent finding that the proton donor to the active site is the side chain of a glutamate residue in Tam HydS,[27] compared to a cysteine residue in Cr HydA1 and other prototypical hydrogenases.[3] The other explanation applies if the rate constant of H_2 binding at the active site is smaller than the (de)protonation rate constants. In that case, K_3 equates k_{-1}^{max}/k_1^{max} K_{relay}, which is the acidity constant of the doubly reduced catalytic intermediate (cf. Section S2.4), and our analysis suggests that this intermediate is harder to protonate in Tam HydS than in Cr HydA1. This protonation, which is required to close the catalytic cycle, has so far proven challenging to firmly identify in spectroscopic investigations.[16,19]

Overall, our results point to various functional differences between Cr HydA1 and Tam HydS, which all contribute to make the catalytic response of the former more reversible: the lower stability of the half-reduced state (smaller difference between $E_1^{0\prime}$ and $E_2^{0\prime}$, which has not been rationalized yet in terms of active site proteic environment[28]) and the easier protonation of the relay or of the two-electron reduced state (larger pK_3).

We conclude on the consideration, which is clear from eq 25, that the role played by the stabilization of the enzyme−substrate complex ($H_{hyd}H^+$) is decreasing the oxidative catalytic potential and therefore increasing the reversibility of the catalytic signal. An experimental comparison between Cr HydA1 and Tam HydS in this respect is difficult because the Michaelis constants are difficult to measure accurately and impossible to measure and compare at the same temperature. However, eq 25 is another illustration of the idea that flat energy landscapes are not required to obtain a reversible catalytic response:[37,39] that the catalytic cycle that includes high or low energy intermediates may favor reversibility, sometimes at the expense of turnover frequency.

METHODS

The samples of Cr HydA1 and Tam HydS were produced by heterologous expression in *Escherichia coli*, followed by artificial maturation with the $[2Fe]^{adt}$ cofactor as described in references with minor modifications (for details, see the Supporting Information).[25,55,56]

The FTIR measurements were performed in a home-built cell in which a sample of 12 μL of 0.3 mM Cr HydA1 in mixed buffer (20 mM each of acetate, MES, HEPES, Tris, glycine, CAPS) prepared under a 2% H2/98% N2 atm in an anaerobic chamber (Coy) was closed between two CaF_2 windows separated by a 50 μm Teflon spacer. The sample so composed was sealed into the home-built cell with two rubber rings separating the windows from the rest of the housing. The data were recorded in a standard transmission IR spectrometer (a Bruker Vertex v80) equipped with a liquid nitrogen cooled mercury−cadmium-telluride (MCT) detector.

All the electrochemistry experiments were carried out in a Jacomex glovebox filled with nitrogen. The three-electrode electrochemical setup was described in ref 57. The electrochemical cell solution was continuously flushed with either pure H_2 or a mixture of H_2 and Ar adjusted to the desired composition using mass flow controllers (SLA5850S from BROOKS Instruments). The resulting H_2

https://doi.org/10.1021/jacs.3c10693
J. Am. Chem. Soc. 2024, 146, 1455−1466

concentration was calculated from the H_2 partial pressure assuming a solubility of 0.89 mM/atm at 5 °C and 0.64 mM/atm at 40 °C.[58,59]

The films of Cr HydA1 on PGE electrodes were prepared by letting adsorb 0.5 μL of enzyme solution (5−20 μM) for about 3 min, after having polished the electrode surface (~0.1 cm^2) with 1 μm aqueous alumina slurry. The films of Tam HydS were prepared by polishing the electrode surface with 1 μm aqueous alumina slurry and P1200 sandpaper. After sonication, 1 μL of enzyme solution (5−10 μM) was painted on the electrode surface together with 1 μL of polymyxin B sulfate (2−20 mg/mL) and let dry for 5−10 min. The platinized electrode to measure the H^+/H_2 equilibrium potential during the Tam HydS experiments was prepared according to the protocol in ref 60.

All of the electrochemical experiments were performed in a chloride-free mixed buffer: MES, CHES, HEPES, TAPS, Na acetate (all 5 mM), and Na_2SO_4 (0.1 M).

All potentials were measured with respect to a saturated calomel electrode and then corrected for the SHE by using $E_{SHE} = E_{SCE} + 241$ mV.

We accounted for film loss during the series of voltammograms by always recording one CV at pH 7 or at 1 mM [H_2] between every experiment at a different pH or H_2 pressure, respectively, and normalizing the limiting currents (as, e.g., in ref 61). Only in the series of experiments with Tam HydS as a function of pH was this not necessary because the films were very stable. The capacitive current was removed by subtracting a blank recorded with no enzyme, and the forward and backward sweeps averaged.

The data were analyzed using the Qsoas software, available at www.qsoas.org.[62]

■ ASSOCIATED CONTENT

Supporting Information

The Supporting Information is available free of charge at https://pubs.acs.org/doi/10.1021/jacs.3c10693.

Additional experimental details, materials, and methods regarding the experiment in Figure 2; additional kinetic models and their discussions; fits of E_{cat} and i_{lim} as a function of pH at 5 °C for Cr HydA1; Tam HydS K_M measurement; analysis of the cyclic voltammograms of Cr HydA1 and Tam HydS recorded under various conditions; and preparation of [2Fe]ADT-activated Tam HydS (PDF)

■ AUTHOR INFORMATION

Corresponding Author

Christophe Léger − *Laboratoire de Bioénergétique et Ingénierie des Protéines. CNRS, Aix Marseille Université, UMR, 7281 Marseille, France;* orcid.org/0000-0002-8871-6059; Email: chistophe.leger@imm.cnrs.fr

Authors

Andrea Fasano − *Laboratoire de Bioénergétique et Ingénierie des Protéines. CNRS, Aix Marseille Université, UMR, 7281 Marseille, France;* orcid.org/0000-0002-8322-1620

Carole Baffert − *Laboratoire de Bioénergétique et Ingénierie des Protéines. CNRS, Aix Marseille Université, UMR, 7281 Marseille, France*

Conrad Schumann − *Molecular Biomimetics, Department of Chemistry, Ångström Laboratory, Uppsala University, 75120 Uppsala, Sweden;* orcid.org/0009-0007-0847-1420

Gustav Berggren − *Molecular Biomimetics, Department of Chemistry, Ångström Laboratory, Uppsala University, 75120 Uppsala, Sweden;* orcid.org/0000-0002-6717-6612

James A. Birrell − *School of Life Sciences, University of Essex, Colchester CO4 3SQ, U.K.;* orcid.org/0000-0002-0939-0573

Vincent Fourmond − *Laboratoire de Bioénergétique et Ingénierie des Protéines. CNRS, Aix Marseille Université, UMR, 7281 Marseille, France;* orcid.org/0000-0001-9837-6214

Complete contact information is available at: https://pubs.acs.org/10.1021/jacs.3c10693

Notes

The authors declare no competing financial interest.

■ ACKNOWLEDGMENTS

This research was funded by the Centre National de la Recherche Scientifique, Aix Marseille Université, Agence Nationale de la Recherche (ANR-21-21-CE50-0041), Région Sud. This work received support from the French government under the France 2030 investment plan, as part of the Initiative d'Excellence d'Aix-Marseille Université—A*MIDEX, AMX-22-RE-AB-097, G.B. and C.S. gratefully acknowledge the financial support from the European Union Horizon Europe—the Framework Programme for Research and Innovation (2021−2027) under the grant agreement number 101070948 (project PhotoSynH2). The authors are very grateful to Frédérique Berger, glass blower at Aix Marseille University. The FrenchBIC CNRS network (www.frenchbic.cnrs.fr) supported A.F.'s stay in Mulheim to perform the FTIR experiments.

■ REFERENCES

(1) Silakov, A.; Wenk, B.; Reijerse, E.; Lubitz, W. ^{14}N HYSCORE Investigation of the H-cluster of [FeFe] Hydrogenase: Evidence for a Nitrogen in the Dithiol Bridge. *Phys. Chem. Chem. Phys.* **2009**, *11* (31), 6592−6599.

(2) Berggren, G.; Adamska, A.; Lambertz, C.; Simmons, T. R.; Esselborn, J.; Atta, M.; Gambarelli, S.; Mouesca, J. M.; Reijerse, E.; Lubitz, W.; Happe, T.; Artero, V.; Fontecave, M. Biomimetic Assembly and Activation of [FeFe]-Hydrogenases. *Nature* **2013**, *499* (7456), 66−69.

(3) Duan, J.; Senger, M.; Esselborn, J.; Engelbrecht, V.; Wittkamp, F.; Apfel, U.-P.; Hofmann, E.; Stripp, S. T.; Happe, T.; Winkler, M. Crystallographic and Spectroscopic Assignment of the Proton Transfer Pathway in [FeFe]-Hydrogenases. *Nat. Commun.* **2018**, *9* (1), 4726.

(4) Cornish, A. J.; Gärtner, K.; Yang, H.; Peters, J. W.; Hegg, E. L. Mechanism of Proton Transfer in [FeFe]-Hydrogenase from *Clostridium pasteurianum*. *J. Biol. Chem.* **2011**, *286* (44), 38341−38347.

(5) Greening, C.; Biswas, A.; Carere, C. R.; Jackson, C. J.; Taylor, M. C.; Stott, M. B.; Cook, G. M.; Morales, S. E. Genomic and Metagenomic Surveys of Hydrogenase Distribution Indicate H_2 is a Widely Utilised Energy Source for Microbial Growth and Survival. *ISME J.* **2016**, *10* (3), 761−777.

(6) Birrell, J. A.; Rodríguez-Maciá, P.; Reijerse, E. J.; Martini, M. A.; Lubitz, W. The Catalytic Cycle of [FeFe] Hydrogenase: A Tale of Two Sites. *Coord. Chem. Rev.* **2021**, *449*, 214191.

(7) Lorent, C.; Katz, S.; Duan, J.; Kulka, C. J.; Caserta, G.; Teutloff, C.; Yadav, S.; Apfel, U.-P.; Winkler, M.; Happe, T.; Horch, M.; Zebger, I. Shedding Light on Proton and Electron Dynamics in [FeFe] Hydrogenases. *J. Am. Chem. Soc.* **2020**, *142* (12), 5493−5497.

(8) Sommer, C.; Adamska-Venkatesh, A.; Pawlak, K.; Birrell, J. A.; Rüdiger, O.; Reijerse, E. J.; Lubitz, W. Proton Coupled Electronic Rearrangement within the H-cluster as an Essential Step in the Catalytic Cycle of [FeFe] Hydrogenases. *J. Am. Chem. Soc.* **2017**, *139* (4), 1440−1443.

(9) Laun, K.; Baranova, I.; Duan, J.; Kertess, L.; Wittkamp, F.; Apfel, U.-P.; Happe, T.; Senger, M.; Stripp, S. T. Site-Selective Protonation of the One-Electron Reduced Cofactor in [FeFe]-Hydrogenase. *Dalton Trans.* **2021**, *50* (10), 3641−3650.

(10) Roseboom, W.; De Lacey, A. L.; Fernandez, V. M.; Hatchikian, E. C.; Albracht, S. P. J. The Active Site of the [FeFe]-Hydrogenase from *Desulfovibrio desulfuricans*. II. Redox Properties, Light Sensitivity and CO-Ligand Exchange as Observed by Infrared Spectroscopy. *J. Biol. Inorg. Chem.* **2006**, *11* (1), 102−118.
(11) Mebs, S.; Senger, M.; Duan, J.; Wittkamp, F.; Apfel, U.-P.; Happe, T.; Winkler, M.; Stripp, S. T.; Haumann, M. Bridging Hydride at Reduced H-cluster Species in [FeFe]-Hydrogenases Revealed by Infrared Spectroscopy, Isotope Editing, and Quantum Chemistry. *J. Am. Chem. Soc.* **2017**, *139* (35), 12157−12160.
(12) Ratzloff, M. W.; Artz, J. H.; Mulder, D. W.; Collins, R. T.; Furtak, T. E.; King, P. W. CO-Bridged H-cluster Intermediates in the Catalytic Mechanism of [FeFe]-Hydrogenase CaI. *J. Am. Chem. Soc.* **2018**, *140* (24), 7623−7628.
(13) Birrell, J. A.; Pelmenschikov, V.; Mishra, N.; Wang, H.; Yoda, Y.; Tamasaku, K.; Rauchfuss, T. B.; Cramer, S. P.; Lubitz, W.; DeBeer, S. Spectroscopic and Computational Evidence That [FeFe] Hydrogenases Operate Exclusively with CO-Bridged Intermediates. *J. Am. Chem. Soc.* **2020**, *142* (1), 222−232.
(14) Adamska, A.; Silakov, A.; Lambertz, C.; Rüdiger, O.; Happe, T.; Reijerse, E.; Lubitz, W. Identification and Characterization of the "Super-Reduced" State of the H-cluster in [FeFe] Hydrogenase: A New Building Block for the Catalytic Cycle? *Angew. Chem. Int. Ed.* **2012**, *51* (46), 11458−11462.
(15) Pelmenschikov, V.; Birrell, J. A.; Pham, C. C.; Mishra, N.; Wang, H.; Sommer, C.; Reijerse, E.; Richers, C. P.; Tamasaku, K.; Yoda, Y.; Rauchfuss, T. B.; Lubitz, W.; Cramer, S. P. Reaction Coordinate Leading to H_2 Production in [FeFe]-Hydrogenase Identified by Nuclear Resonance Vibrational Spectroscopy and Density Functional Theory. *J. Am. Chem. Soc.* **2017**, *139* (46), 16894−16902.
(16) Mulder, D. W.; Ratzloff, M. W.; Bruschi, M.; Greco, C.; Koonce, E.; Peters, J. W.; King, P. W. Investigations on the Role of Proton-Coupled Electron Transfer in Hydrogen Activation by [FeFe]-Hydrogenase. *J. Am. Chem. Soc.* **2014**, *136* (43), 15394−15402.
(17) Mulder, D. W.; Guo, Y.; Ratzloff, M. W.; King, P. W. Identification of a Catalytic Iron-Hydride at the H-Cluster of [FeFe]-Hydrogenase. *J. Am. Chem. Soc.* **2017**, *139* (1), 83−86.
(18) Rumpel, S.; Sommer, C.; Reijerse, E.; Farès, C.; Lubitz, W. Direct Detection of the Terminal Hydride Intermediate in [FeFe] Hydrogenase by NMR Spectroscopy. *J. Am. Chem. Soc.* **2018**, *140* (11), 3863−3866.
(19) Mészáros, L. S.; Ceccaldi, P.; Lorenzi, M.; Redman, H. J.; Pfitzner, E.; Heberle, J.; Senger, M.; Stripp, S. T.; Berggren, G. Spectroscopic Investigations under Whole-Cell Conditions Provide New Insight into the Metal Hydride Chemistry of [FeFe]-Hydrogenase. *Chem. Sci.* **2020**, *11* (18), 4608−4617.
(20) Senger, M.; Laun, K.; Wittkamp, F.; Duan, J.; Haumann, M.; Happe, T.; Winkler, M.; Apfel, U.-P.; Stripp, S. T. Proton-Coupled Reduction of the Catalytic [4Fe-4S] Cluster in [FeFe]-Hydrogenases. *Angew. Chem. Int. Ed.* **2017**, *56* (52), 16503−16506.
(21) Rodríguez-Maciá, P.; Breuer, N.; DeBeer, S.; Birrell, J. A. Insight into the Redox Behavior of the [4Fe−4S] Subcluster in [FeFe] Hydrogenases. *ACS Catal.* **2020**, *10* (21), 13084−13095.
(22) Martini, M. A.; Rüdiger, O.; Breuer, N.; Nöring, B.; DeBeer, S.; Rodríguez-Maciá, P.; Birrell, J. A. The Nonphysiological Reductant Sodium Dithionite and [FeFe] Hydrogenase: Influence on the Enzyme Mechanism. *J. Am. Chem. Soc.* **2021**, *143* (43), 18159−18171.
(23) Senger, M.; Duan, J.; Pavliuk, M. V.; Apfel, U.-P.; Haumann, M.; Stripp, S. T. Trapping an Oxidized and Protonated Intermediate of the [FeFe]-Hydrogenase Cofactor under Mildly Reducing Conditions. *Inorg. Chem.* **2022**, *61* (26), 10036−10042.
(24) Chongdar, N.; Birrell, J. A.; Pawlak, K.; Sommer, C.; Reijerse, E. J.; Rüdiger, O.; Lubitz, W.; Ogata, H. Unique Spectroscopic Properties of the H-Cluster in a Putative Sensory [FeFe] Hydrogenase. *J. Am. Chem. Soc.* **2018**, *140* (3), 1057−1068.
(25) Land, H.; Sekretareva, A.; Huang, P.; Redman, H. J.; Németh, B.; Polidori, N.; Mészáros, L. S.; Senger, M.; Stripp, S. T.; Berggren, G. Characterization of a Putative Sensory [FeFe]-Hydrogenase Provides New Insight into the Role of the Active Site Architecture. *Chem. Sci.* **2020**, *11* (47), 12789−12801.
(26) Calusinska, M.; Happe, T.; Joris, B.; Wilmotte, A. The Surprising Diversity of Clostridial Hydrogenases: A Comparative Genomic Perspective. *Microbiology* **2010**, *156* (6), 1575−1588.
(27) Cabotaje, P. R.; Walter, K.; Zamader, A.; Huang, P.; Ho, F.; Land, H.; Senger, M.; Berggren, G. Probing Substrate Transport Effects on Enzymatic Hydrogen Catalysis: An Alternative Proton Transfer Pathway in Putatively Sensory [FeFe] Hydrogenase. *ACS Catal.* **2023**, *13* (15), 10435−10446.
(28) Chongdar, N.; Rodríguez-Maciá, P.; Reijerse, E. J.; Lubitz, W.; Ogata, H.; Birrell, J. A. Redox Tuning of the H-cluster by Second Coordination Sphere Amino Acids in the Sensory [FeFe] Hydrogenase from *Thermotoga maritima*. *Chem. Sci.* **2023**, *14* (13), 3682−3692.
(29) Armstrong, F. A.; Hirst, J. Reversibility and Efficiency in Electrocatalytic Energy Conversion and Lessons from Enzymes. *Proc. Natl. Acad. Sci. U.S.A.* **2011**, *108* (34), 14049−14054.
(30) Dutta, A.; Appel, A. M.; Shaw, W. J. Designing Electrochemically Reversible H2 Oxidation and Production Catalysts. *Nat. Rev. Chem.* **2018**, *2* (9), 244−252.
(31) Fasano, A.; Land, H.; Fourmond, V.; Berggren, G.; Léger, C. Reversible or Irreversible Catalysis of H+/H2 Conversion by FeFe Hydrogenases. *J. Am. Chem. Soc.* **2021**, *143* (48), 20320−20325.
(32) Fourmond, V.; Plumeré, N.; Léger, C. Reversible Catalysis. *Nat. Rev. Chem.* **2021**, *5* (5), 348−360.
(33) Léger, C.; Bertrand, P. Direct Electrochemistry of Redox Enzymes as a Tool for Mechanistic Studies. *Chem. Rev.* **2008**, *108* (7), 2379−2438.
(34) Sensi, M.; del Barrio, M.; Baffert, C.; Fourmond, V.; Léger, C. New Perspectives in Hydrogenase Direct Electrochemistry. *Curr. Opin. Electrochem.* **2017**, *5* (1), 135−145.
(35) Fourmond, V.; Baffert, C.; Sybirna, K.; Lautier, T.; Abou Hamdan, A.; Dementin, S.; Soucaille, P.; Meynial-Salles, I.; Bottin, H.; Léger, C. Steady-State Catalytic Wave-Shapes for 2-Electron Reversible Electrocatalysts and Enzymes. *J. Am. Chem. Soc.* **2013**, *135* (10), 3926−3938.
(36) Savéant, J. M. Molecular Catalysis of Electrochemical Reactions. Cyclic Voltammetry of Systems Approaching Reversibility. *ACS Catal.* **2018**, *8* (8), 7608−7611.
(37) Fourmond, V.; Wiedner, E. S.; Shaw, W. J.; Léger, C. Understanding and Design of Bidirectional and Reversible Catalysts of Multielectron, Multistep Reactions. *J. Am. Chem. Soc.* **2019**, *141* (28), 11269−11285.
(38) Costentin, C. Molecular Catalysis of Electrochemical Reactions. Overpotential and Turnover Frequency: Unidirectional and Bidirectional Systems. *ACS Catal.* **2021**, *11* (9), 5678−5687.
(39) Reuillard, B.; Costentin, C.; Artero, V. Deciphering Reversible Homogeneous Catalysis of the Electrochemical H_2 Evolution and Oxidation: Role of Proton Relays and Local Concentration Effects. *Angew. Chem. Int. Ed.* **2023**, *62* (36), No. e202302779.
(40) Fasano, A.; Fourmond, V.; Léger, C. Kinetic Modeling of $2e^-/1H^+$ and $2e^-/2H^+$ Bidirectional Catalytic Cycles. *Bioelectrochemistry* **2024**, *155*, 108511.
(41) Fourmond, V.; Léger, C. Modelling the Voltammetry of Adsorbed Enzymes and Molecular Catalysts. *Curr. Opin. Electrochem.* **2017**, *1* (1), 110−120.
(42) Léger, C.; Jones, A. K.; Albracht, S. P. J.; Armstrong, F. A. Effect of a Dispersion of Interfacial Electron Transfer Rates on Steady State Catalytic Electron Transport in [NiFe]-Hydrogenase and Other Enzymes. *J. Phys. Chem. B* **2002**, *106* (50), 13058−13063.
(43) Hirst, J.; Duff, J. L. C.; Jameson, G. N. L.; Kemper, M. A.; Burgess, B. K.; Armstrong, F. A. Kinetics and Mechanism of Redox-Coupled, Long-Range Proton Transfer in an Iron−Sulfur Protein. Investigation by Fast-Scan Protein-Film Voltammetry. *J. Am. Chem. Soc.* **1998**, *120* (28), 7085−7094.

https://doi.org/10.1021/jacs.3c10693
J. Am. Chem. Soc. 2024, 146, 1455−1466

(44) Butt, J. N.; Jeuken, L. J. C.; Zhang, H.; Burton, J. A. J.; Sutton-Cook, A. L. Protein Film Electrochemistry. *Nat. Rev. Methods Primers* **2023**, *3* (1), 77.
(45) Fourmond, V.; Baffert, C.; Sybirna, K.; Dementin, S.; Abou-Hamdan, A.; Meynial-Salles, I.; Soucaille, P.; Bottin, H.; Léger, C. The Mechanism of Inhibition by H_2 of H_2-Evolution by Hydrogenases. *Chem. Commun.* **2013**, *49* (61), 6840−6842.
(46) Domnik, L.; Merrouch, M.; Goetzl, S.; Jeoung, J.-H.; Léger, C.; Dementin, S.; Fourmond, V.; Dobbek, H. CODH-IV: A High-Efficiency CO-Scavenging CO Dehydrogenase with Resistance to O_2. *Angew. Chem. Int. Ed.* **2017**, *56* (48), 15466−15469.
(47) Léger, C.; Heffron, K.; Pershad, H. R.; Maklashina, E.; Luna-Chavez, C.; Cecchini, G.; Ackrell, B. A.; Armstrong, F. A. Enzyme Electrokinetics: Energetics of Succinate Oxidation by Fumarate Reductase and Succinate Dehydrogenase. *Biochemistry* **2001**, *40* (37), 11234−11245.
(48) Meneghello, M.; Uzel, A.; Broc, M.; Manuel, R. R.; Magalon, A.; Léger, C.; Pereira, I. A. C.; Walburger, A.; Fourmond, V. Electrochemical Kinetics Support a Second Coordination Sphere Mechanism in Metal-Based Formate Dehydrogenase. *Angew. Chem. Int. Ed.* **2023**, *62* (6), No. e202212224.
(49) Hajj, V.; Baffert, C.; Sybirna, K.; Meynial-Salles, I.; Soucaille, P.; Bottin, H.; Fourmond, V.; Léger, C. FeFe Hydrogenase Reductive Inactivation and Implication for Catalysis. *Energy Environ. Sci.* **2014**, *7* (2), 715−719.
(50) Megarity, C. F.; Esselborn, J.; Hexter, S. V.; Wittkamp, F.; Apfel, U.-P.; Happe, T.; Armstrong, F. A. Electrochemical Investigations of the Mechanism of Assembly of the Active-Site H-cluster of [FeFe]-Hydrogenases. *J. Am. Chem. Soc.* **2016**, *138* (46), 15227−15233.
(51) Cunningham, D. W.; Barlow, J. M.; Velasquez, R. S.; Yang, J. Reversible and Selective CO_2 to HCO_2^- Electrocatalysis near the Thermodynamic Potential. *Angew. Chem. Int. Ed.* **2020**, *59*, 4443.
(52) Cunningham, D. W.; Yang, J. Y. Kinetic and Mechanistic Analysis of a Synthetic Reversible CO_2/HCO_2^- Electrocatalyst. *Chem. Commun.* **2020**, *56*, 12965−12968.
(53) Dutta, A.; DuBois, D. L.; Roberts, J. A. S.; Shaw, W. J. Amino Acid Modified Ni Catalyst Exhibits Reversible H_2 Oxidation/production over a Broad pH Range at Elevated Temperatures. *Proc. Natl. Acad. Sci. U.S.A.* **2014**, *111* (46), 16286−16291.
(54) Hessin, C.; Schleinitz, J.; Le Breton, N.; Choua, S.; Grimaud, L.; Fourmond, V.; Desage-El Murr, M.; Léger, C. Assessing the Extent of Potential Inversion by Cyclic Voltammetry: Theory, Pitfalls, and Application to a Nickel Complex with Redox-Active Iminosemiquinone Ligands. *Inorg. Chem.* **2023**, *62* (8), 3321−3332.
(55) Kuchenreuther, J. M.; Grady-Smith, C. S.; Bingham, A. S.; George, S. J.; Cramer, S. P.; Swartz, J. R. High-Yield Expression of Heterologous [FeFe] Hydrogenases in *Escherichia coli*. *PLoS One* **2010**, *5* (11), No. e15491.
(56) Esselborn, J.; Lambertz, C.; Adamska-Venkatesh, A.; Simmons, T.; Berggren, G.; Noth, J.; Siebel, J.; Hemschemeier, A.; Artero, V.; Reijerse, E.; Fontecave, M.; Lubitz, W.; Happe, T. Spontaneous Activation of [FeFe]-Hydrogenases by an Inorganic [2Fe] Active Site Mimic. *Nat. Chem. Biol.* **2013**, *9* (10), 607−609.
(57) Léger, C.; Dementin, S.; Bertrand, P.; Rousset, M.; Guigliarelli, B. Inhibition and Aerobic Inactivation Kinetics of *Desulfovibrio fructosovorans* NiFe Hydrogenase Studied by Protein Film Voltammetry. *J. Am. Chem. Soc.* **2004**, *126* (38), 12162−12172.
(58) Morrison, T. J.; Billett, F. 730. The salting-out of non-electrolytes. Part II. The effect of variation in non-electrolyte. *J. Chem. Soc.* **1952**, 3819−3822.
(59) Morrison, T. J. 729. The salting-out of non-electrolytes. Part I. The effect of ionic size, ionic charge, and temperature. *J. Chem. Soc.* **1952**, 3814−3818.
(60) White, S. F.; Turner, A. P. F.; Schmid, R. D.; Bilitewski, U. Investigations of Platinized and Rhodinized Carbon Electrodes for Use in Glucose Sensors. *Electroanalysis* **1994**, *6*, 625.
(61) Léger, C.; Jones, A. K.; Roseboom, W.; Albracht, S. P. J.; Armstrong, F. A. Enzyme Electrokinetics: Hydrogen Evolution and Oxidation by *Allochromatium vinosum* [NiFe]-Hydrogenase. *Biochemistry* **2002**, *41* (52), 15736−15746.
(62) Fourmond, V. QSoas: A Versatile Software for Data Analysis. *Anal. Chem.* **2016**, *88* (10), 5050−5052.

https://doi.org/10.1021/jacs.3c10693
J. Am. Chem. Soc. 2024, 146, 1455−1466